Journal of Mining and Environment (JME), Vol. 14, No. 4, 2023, 1261-1272

Shahrood University of Technology

Journal of Mining and Environment (JME)

Journal homepage: www.jme.shahroodut.ac.ir

Iranian Society of Mining Engineering (IRSME)

Permeability Tensor Calculation of Pumped Storage Power Plant Cavern of Rudbar Lorestan Dam using Crack Tensor

Akbar Esmaeilzadeh[1*], Kourosh Shahriar[2], and Reza Mikaeil[1]

1. Department of Mining Engineering, Environment Faculty, Urmia University of Technology, Urmia, Iran
2. Mining Department, Mining and Metallurgical Faculty, AmirKabir University of Technology, Tehran, Iran

Article Info

Received 8 February 2023
Received in Revised form 24 July 2023
Accepted 7 August 2023
Published online 7 August 2023

DOI: 10.22044/jme.2023.12637.2298

Keywords

Crack Tensor
Permeability Tensor
Pumped Storage
Power Plant
Rudbar Lorestan

Abstract

The hydraulic properties of the rock masses are of great importance in analyzing the behavior and stability of the structures constructed on or in rock mass. Permeability is key parameter among other rock mass features due to its important role in rock mass overall behavior. According to aforementioned reason, numerous efforts have been made by researchers in the field of rock mechanics for its obtaining. To access the rock masses' permeability, in-situ test methods and simulation techniques could be used. In-situ tests like Lugeon Test are time-consuming and costly and they provide local results. Simulation base methods calculate the permeability of the model that is generated similar to the real region indeed and the developing the results to the real condition always raises substantial challenges. According to the aforementioned reason, direct acquiring of permeability with optimum cost and time which is easily generalizable to the overall of a region would be very important. In this work using crack tensor concept, permeability tensor of Lorestan's Rudbar dam cavern is calculated efficiently by considering rock mass structural features. Resulted permeability of the power plant's cavern was obtained equal to $11.220 \times 10^{-7}\ \frac{m}{s}$ that seems to be acceptable compared to the measured values which is obtained$9.87 \times 10^{-7}\ \frac{m}{s}$.

1. Introduction

The stability of the structures constructed in or on the rock masses predominantly depends on the presence of the fractures in the structure of the rock mass [1]. Fractures presence in structure of rock change behavior of it in a way that it seems rock mass and intact rock are different materials. The exact determination of the mechanical properties of the rock mass is a vital issue for reaching a safe and economic design for the spaces created in or on the rock mass [2–5]. The complex fracture patterns, and their statistical nature and uncertainties in describing geo-mechanically and geometrically characteristics of the fractured rock masses have transformed them into the complex and hard constructional materials. It is clearly evident that the geometry of the fractures should play an important role in the study of the rock mass's anisotropy [6]. The studies are reflective of the high importance of fractures in the permeability of the fluids into the rock mass and it is for the same reason that permeability has been taken into account in solving the problems related to geothermal energy, seismology, dumping of the hazardous radioactive waste [7–10].

The determination of the hydraulic specifications of rock mass has drawn the attentions of many researchers due to being of a great importance. The equivalent permeability of the rock mass is considered among the most important entries in the discussions on the calculation of water leakage and discharge into the underground spaces. It has to be explicitly mentioned that the fluid flow into the rock mass occurs in the majority of the cases through the joints, stratification and foliation.

✉ *Corresponding author: a.esmailzadeh@uut.ac.ir (A. Esmaeilzadeh)*

Liakopoulos calculated the anisotropic homogeneous soil's permeability in the form of a positive, symmetrical and second order tensor [11]. Greenkorn *et al.* and Asadi *et al.* studied the anisotropic permeability based on a laboratory method and offered methods for calculating the main indicators of permeability but they have not mentioned anything about the calculation of permeability tensor [12, 13]. Long *et al.*, Min *et al.*, and Zhang *et al.* have used the discrete discontinuity network for calculating and simulating the flows inside the discontinuities[14–16]. Based on the certainty of the geometrical properties of the discontinuities and their joint patterns, they performed the simulation process. Hestir and Lang, De Dreuzy *et al.* applied a combination of percolation and discrete discontinuity network theories for obtaining permeability [17, 18]. Zimmerman and Bodvarsson simulated each fracture as a conductive element that conductivity of which depended on the hydraulic opening of the discontinuity and subsequently used the simulation results for computing the 2D permeability of the fractured rocks [19]. To determine the equivalent permeability tensor of the rock mass, Snow and Zhou *et al.* offered completely analytical methods based on the geometrical properties of the joint network. Oda applied statistical methods to come up with a method for determining permeability tensor. The first effort for calculating permeability tensor was made by Snow who assumed an unlimited number of joints in doing so. Firstly, he calculated the equivalent rock mass permeability tensor for a single-point discontinuity and subsequently applied Principle of superposition to obtain the permeability tensor for the joint network [19]. It was Snow who for the first time considered a simple but understandable model for evaluating the permeability rate based on the concept of the flow between parallel plates and offered fractures' pattern through taking some statistical considerations into account [20]. In comparison to the Snow's model, Bear performed simplifications and considered soft surfaces for the fractures' walls to offer a better model for fluid flow that was confirmed by Witherspoon *et al.* in laboratory [20].

Kiraly *et al.* offered a similar relation which in case of using limited plates for discontinuities, take into account the number of discontinuities that be exactly the same as the number of the joints inside the rock mass so that the equivalent permeability tensor could be calculated with an acceptable accuracy [21]. Rocha *et al.* conducted field studies to improve the tensor calculated based on Snow's theory. They considered a well and measured the flow therein and subsequently offered a revised coefficient by dividing it by the flow calculated by Snow [22]. Zoorabadi *et al.* offered a new method for calculating the permeability tensor for the non-ductile discrete discontinuity network [23]. Pan et al. constructed the fracture network and calculated the fractures tensor followed by calculation of the permeability to take an important step in using fracture tensor concept in analyzing the hydraulic behavior of the rock mass [24]. Rutqvist *et al.* offered the concept of interconnected continuous environments thereby to come up with a novel method of estimating the hydraulic characteristics of the rock mass that uses fracture tensor [25].

Oda introduced the crack tensor concept. The studies are reflective of the importance of fractures geometry effect on the rock mass permeability. Permeability tensor is an injective function of fracture tensor and also the main directions of permeability are in fact aligned with the main directions of crack tensor. Fracture tensor is most frequently applied in such areas as geotechnics, environment, and civil engineering, especially in estimating the rock mass permeability or hydraulic conductivity [4].

The notable issue that shows the importance of using fracture tensor in calculating the permeability tensor is that the rock masses hydraulic characteristics have been calculated in all of the abovementioned studies based on parameters that do not incorporate the geometrical properties of the fractures and, in other words, the hydraulic computations and, more explicitly, the permeability tensor calculations have been carried out without direct interference of the fractures geometrical specifications [26]. On the other hand, there is a need for reproduction of a fracture network in the above-cited methods that can be used for taking the later stages for the reproduced network's calculations so as to figure out how much it is matching with the real conditions and this is a vague question. In fact, the hydraulic conditions of the model which is simulated the real region are calculated in the majority of the cases instead of computing the permeability tensor of the region. On the other hand, in most of the proposed methods that calculate permeability tensor without using the fracture tensor, a simulation of region is firstly generated and hydraulic parameters is computed for the model. It is notable that regeneration of the region's fracture model is time-consuming, costly, and prone to errors process [26].

Using the process of fracture tensor calculation and, subsequently, calculation of the permeability tensor using it, make enables the consideration of direct role of fractures geometrical properties in calculation process and the calculated permeability tensor is obtained for the studied region itself and not for the simulated model and thus there would be no need for the difficult and time-consuming and, of course, error-prone process of creating a fracture network model for the studied region, as well. In this work, the data collected from the site of Rudbar Lorestan pumped storage power plant cavern will be used to calculate region's fracture tensor and then permeability tensor will be calculated using fracture tensor.

2. Site Investigation

The data obtained from the cavern of pumped-storage power plant of Rudbar Lorestan dam. Rudbar, Lorestan pumped storage plant located in high Zagros zone has very complicated tectonic conditions and numerous over thrust faults. The active faults of Saravan Baznavid and Chaleh Hatam are the most important faults in the site. The carven of the power plant is located almost in the center of an anticline. The cavern has a length of 130 meters, a width of 26 meters and a height of 50 meters (Figure 1), located in the Dalan Formation (end of the first geology period), with calcareous rock masses and dolomitic limestone of average thickness (Figure 2). This project is under construction at the Rudbar Lorestan Dam upstream, located 150 km west of Isfahan and 100 km south of Aligudarz city. The area of the project is located under the sedimentary zone (internal Zagros) (Figure 3).

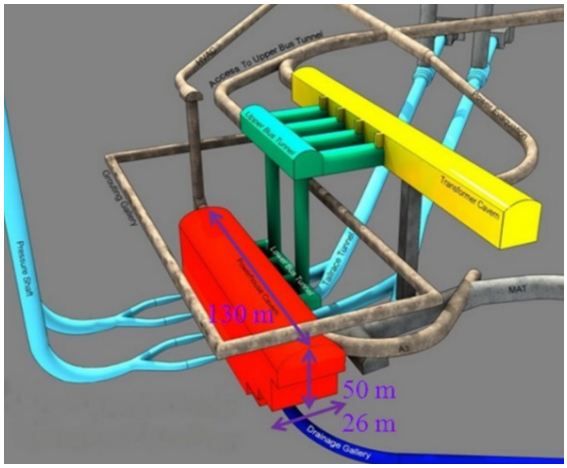

Figure 1. Layout of cavern of pumped-storage power plant project of Rudbar, Lorestan dam.

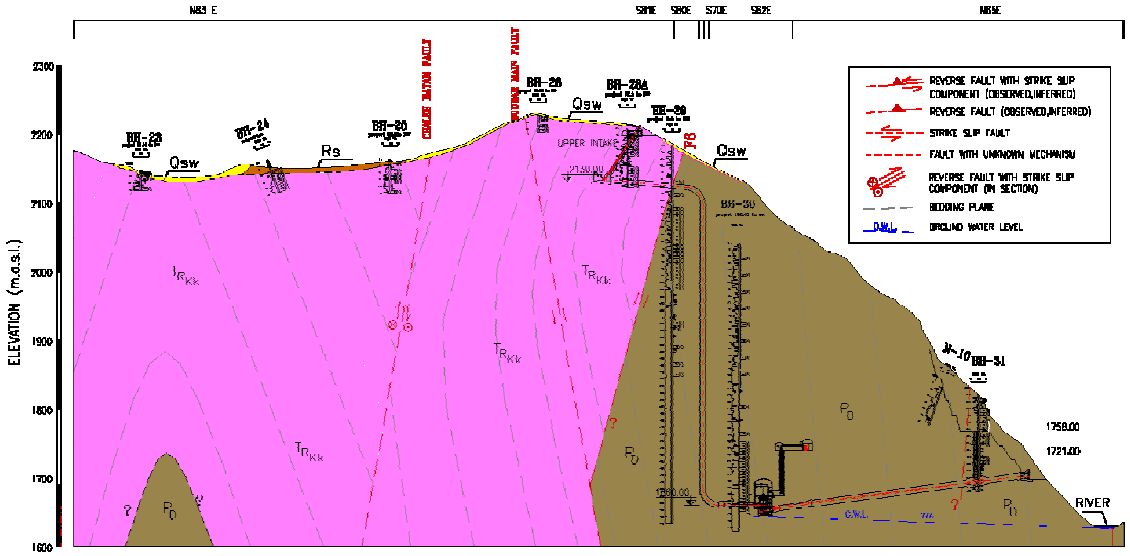

Figure 2. Geology cross-section of pumped-storage power plant project of Rudbar, Lorestan dam.

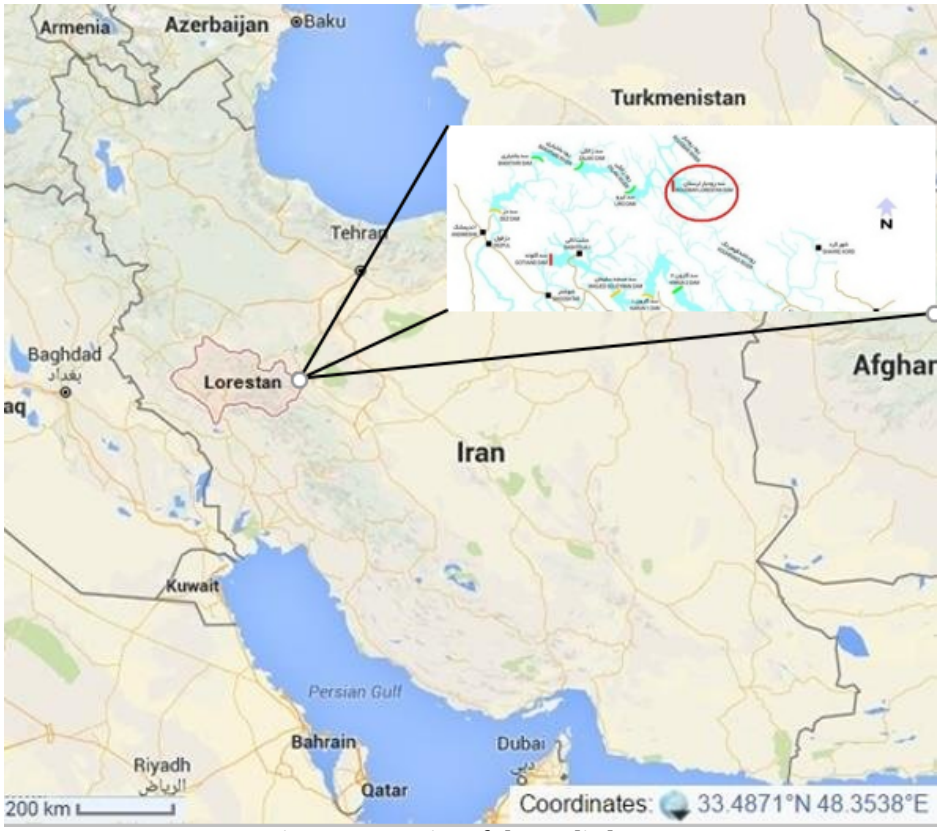

Figure 3. Location of the studied area.

The data is obtained from the cavern by scanline and scan window surveying method, and its number reaches 627 fractures.

3. Methodology

Use of the fractures geometrical characteristics in calculating the permeability tensor is a very important aspect of the hydraulic calculations but it has been neglected in the majority of the calculation methods. Besides performing the calculations using the directly collected field data, calculation of the permeability tensor using the crack tensor method takes the fractures geometrical characteristics into account. The permeability tensor calculation process using crack tensor has been explained in following.

A volume of the rock mass equal to V is considered as the flow region. Flow region has been homogeneously intersected by $m^{(v)}$ number of discontinuities which their centers have been distributed randomly in volume V. The discontinuities are elliptical in shape with its large diameter being of the size α and the diameters ratio of k and an opening of t. Therefore, the void volume corresponding to each crack equals $(\pi/4)(a^2/k)t$. The crack orientation is shown by two normal vectors of $n^{(-)}$ and $n^{(+)}$ that are perpendicular to the crack plate (Figure 4).

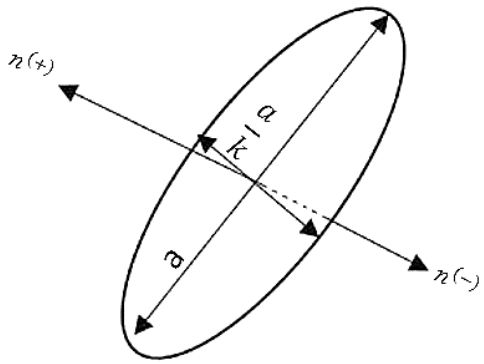

Figure 4. Illustration of normal unit vectors of elliptical joint.

It is worth to mention that $n^{(+)}$ is along $n^{(-)}$ but in an opposite direction. Here, n denotes $n^{(+)}$ and $n^{(-)}$ and it is considered as part of the spatial angle of Ω that is defined on a sphere with a unit radius. The rock mass is assumed with an impermeable matrix. Thus, the fluid can only pass through the cracks. Under the abovementioned conditions, the

apparent velocity of the fluid current, $\overline{v_i}$, is defined in the form of the relation:

$$\overline{v_i} = \frac{1}{V}\int_V v_i dV = \frac{1}{V}\int_{V^{(c)}} v_i^{(c)} dV^{(c)} \quad (1)$$

$v_i^{(c)}$: Local velocity in cracks

$V^{(c)}$: Void volume in crack canal

It is assumed that the normal unit vector of the cracks is situated in the area of $d\Omega$ spatial angle about *n* and the large diameter of the crack is oval and in the extent of α to α+dα and the cracks' openings are in the extent of t to t+dt. Now, the probability density function, E(n,α,t), is defined in such a way that $2E(n,a,t)d\Omega dadt$ gives a probability value of (n,a,t) for the cracks. In other words, it can be written that as Equation (2):

$$\int_0^\infty \int_0^\infty \int_{\Omega/2} 2E(n,a,t)d\Omega dadt = \int_0^\infty \int_0^\infty \int_\Omega E(n,a,t)d\Omega dadt = 1 \quad (2)$$

In the above relation $\Omega/2$ is half the spatial angle Ω. It is worth mentioning that the maximum size of the main diameter of the ovals and opening, situated in the volume range V, is replaced in the above equation for the infinite expressions. Each crack also creates two-unit vectors, $n^{(+)}$ and $n^{(-)}$ that are in opposite directions to one another. Thus $(n,a,t)d\Omega drdt$, in fact, gives the normal crack vector's probability and not the normal crack vector itself. In this state, the function $E(n,a,t)$ is defined on the spatial angle Ω. Assuming that the discontinuity centers have been randomly distributed in the flow region, it can be stated that the crack geometry is completely determined via specifying the density function and the number of cracks. It can be also stated that $E(n,a,t) = E(-n,a,t)$. It is assumed that dN is the number of cracks the centers of which fall inside the flow region V. To estimate the likely number of the aforementioned cracks, dN is multiplied by the total number of $m^{(V)}$ as shown in Relation (3):

$$dN = 2m^{(V)}E(n,a,t)d\Omega drdt \quad (3)$$

Since each crack produces a void volume equal to $(\pi/4)(a^2/k)t$, the total void volume, $dV^{(c)}$, of the corresponding cracks can be calculated by Relation (4):

$$dV^{(c)} = \frac{(\pi)(a^2/k)t}{4} dN = \frac{\pi m^{(V)}}{2} a^2 tE(n,a,t)d\Omega drdt \quad (4)$$

In the next stage, the velocity of the flow is investigated in the cracks. In this state, the flow domain falls on two boundaries under two hydraulic loads of ϕ_1 and ϕ_2 in such a way that $\phi_1 > \phi_2$. The linear hydraulic load ranging from a maximum value of ϕ_1 to a minimum value of ϕ_2 is exerted in the other two boundaries. Thus, the hydraulic gradient, J, is obtained as shown in Relation (5):

$$J = \frac{\phi_1 - \phi_2}{L} p \quad (5)$$

L: Distance between two head sources

p: Unit vector in flow direction

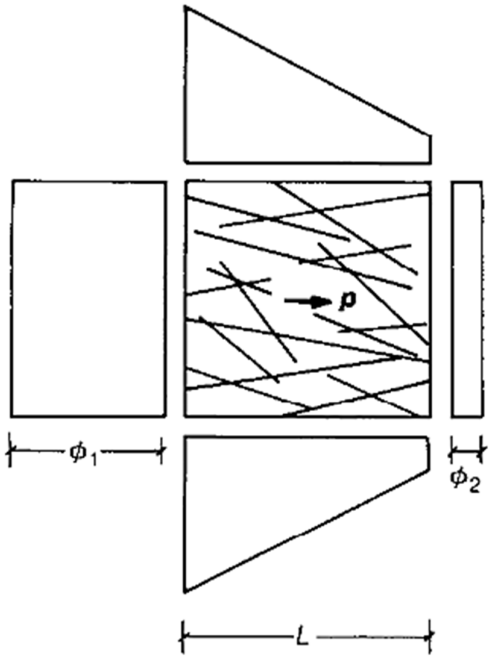

Figure 5. Hydraulic head condition in boundary of DFN.

The head distribution inside the flow domain depends on the hydraulic behavior of the cracks but it is assumed under such conditions that the field gradient is uniform in the entire flow domain. This assumption has been confirmed by Lang *et al.* (1982) based on the permeability analyses of a cracked medium. Of course, it is worth mentioning that this assumption is validated by a sufficient number of cracks. Now, it is assumed that $\boldsymbol{J^{(c)}}$ is the hypothetical indicator of J on the crack:

$$J^{(c)} = J - (n \cdot J)n \tag{6}$$

and/or:

$$J_i^{(c)} = (\delta_{ij} - n_i n_j)J_j \tag{7}$$

δ_{ij}: Kronecker delta

n_i: Projected component of n on reference coordinate set (x_i) ($i = 1, 2, 3$)

J_j: Projected component of J on reference coordinate set (x_i) ($i = 1, 2, 3$)

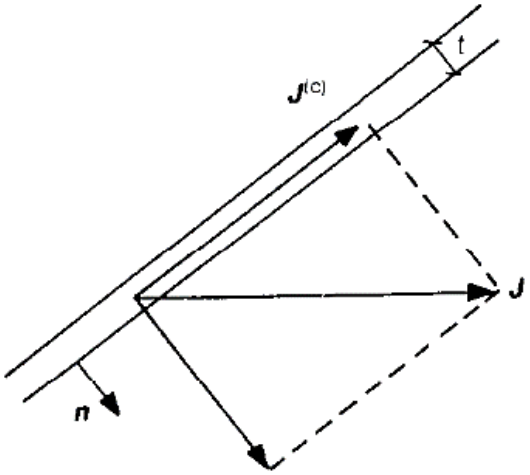

Figure 6. Analysis of vector field of hydraulic gradient on joint plane.

If the crack is found highly propagated, the water would have a layered flow between two parallel plates with an opening equal to t. Under such conditions, the mean velocity of the flow would be equal to Equation (8):

$$v_i^{(c)} = \frac{1}{12}\frac{g}{v}t^2 J_i^{(c)} \tag{8}$$

Now, it can be expected that the cracks would have a flow velocity equal to Equation (9):

$$v_i^{(c)} = \lambda\frac{g}{v}t^2 J_i^{(c)} \tag{9}$$

λ: Dimensionless constant $0 < \lambda \leq 1/12$.

The above constant value tends towards 1.12 with the increase in the crack size. Substituting Relation (7) in Relation (9) gives the apparent fluid velocity in the corresponding cracks as equation (10):

$$v_i^{(c)} = \lambda\frac{g}{v}t^2(\delta_{ij} - n_i n_j)J_j \tag{10}$$

Blending the relations (1), (2), and (10), it can be written that:

$$\overline{v_i} = \frac{1}{V}\int_{V^{(c)}} v_i^{(c)} dV^{(c)} = \lambda\frac{g}{v}\left[\frac{\pi\rho}{4}\int_0^{\infty}\int_0^{\infty}\int_{\Omega} r^2 t^3(\delta_{ij} - n_i n_j) \times E(\boldsymbol{n}, a, t)d\Omega da dt\right]J_i \tag{11}$$

where ρ is the volumetric density of the cracks that is equal to:

*R*elation (11) is integrated on all the cracks within flow domain. Comparison of the relation (6-17) and Darcy relation leads to the permeability tensor calculation relation $k_{ij}^{(c)}$. Thus it can be written:

$$k_{ij}^{(c)} = \lambda(P_{kk}\delta_{ij} - P_{ij}) \tag{12}$$

where:

$$P_{ij} = \frac{\pi\rho}{4}\int_0^{\infty}\int_0^{\infty}\int_{\Omega} r^2 t^3 n_i n_j \times E(\boldsymbol{n}, a, t)\, d\Omega\, da\, dt \qquad (14)$$

and

$$P_{kk} = P_{11} + P_{22} + P_{33} \qquad (13)$$

where P_{ij} is called crack tensor which is a symmetrical second order tensor only related to the geometrical specifications of the discontinuities, including shape, size, opening and orientation. It has to be noted that the above relation has been obtained considering the perfect partitioning of the flow domain by the cracks and there is a large number of paths for flow pass. The final relation gives non-zero values for permeability even when P_{ij} value is trivial while the cracks' connection has reached zero under the above conditions and no flow occurs any more. To overcome this problem, a correction that will be explained below has been made. Crack tensor is multiplied by α that is smaller than unity and this reduces the P_{ij} coefficient in such a way that it is more matched with reality. The threshold limit is observed when $\alpha = \alpha_0$ below which the inter-crack connections are completely removed and the flow domain becomes practically impermeable. Thus the corrective expression, α_{ij}, is determined in such a way that when α_{ij}, it can be stated:

$$k_{ij}^{(c)} = \lambda\left(P_{kk}\delta_{ij} - P_{ij}\right) + \alpha_{ij} \qquad (14)$$

and when $0 < \alpha \leq \alpha_0$, then:

$$k_{ij}^{(c)} = 0 \qquad (15)$$

Since $k_{ij}^{(c)} = 0$ occurs when $\alpha = \alpha_0$, thus it can be stated that:

$$\alpha_{ij} = -\lambda\alpha_0\left(P_{kk}\delta_{ij} - P_{ij}\right) \qquad (16)$$

Replacing Relation (16) in the previous final relation gives the method of calculating the permeability tensor as shown in the following relation:

$$k_{ij}^{(c)} = \lambda(1-\alpha_0)\left(P_{kk}\delta_{ij} - P_{ij}\right) = \lambda\left(\bar{P}_{kk}\delta_{ij} - \bar{P}_{ij}\right) \qquad (17)$$

where:

$$\bar{P}_{ij} = P_{ij} - {P_{ij}}^0 \qquad (18)$$

$${P_{ij}}^0 = \alpha_0 P_{ij} \qquad (19)$$

The value of ${P_{ij}}^0$ would be equal to zero under such conditions that the flow domain is completely partitioned by the cracks. Thus Relation (13) with a value equal to $\lambda = 1.12$ can be applied. Fortunately, the abovementioned conditions predominantly occur in the rock mass as a result of which the rock mass is completely destroyed by the cracks. In other words, the perfect connection conditions are most often available in the nature.

It is assumed that x'_1, x'_2, and x'_3 are the main axes corresponding to the main planes of the tensor P_{ij}. Considering the main axes, the main indicators' matrix of P_{ij} tensor can be diagonally written as below:

$$P_{ij} = \begin{bmatrix} P_1 & 0 & 0 \\ 0 & P_2 & 0 \\ 0 & 0 & P_3 \end{bmatrix} \qquad (20)$$

$$k_{ij}^{(c)} = \begin{bmatrix} k_1^{(c)} & 0 & 0 \\ 0 & k_2^{(c)} & 0 \\ 0 & 0 & k_3^{(c)} \end{bmatrix} \qquad (21)$$

Since $k_{ij}^{(c)}$ is a single-point function of P_{ij} and $\bar{P}_{ij}$, thus its main axes are coaxially aligned with the main axes of crack tensor. Considering i = j, Relation (21) takes the following form:

$$k_{ii}^{(c)} = 2\lambda\bar{P}_{ij} = 2\lambda\left(P_{ii} - {P_{ii}}^0\right) \qquad (22)$$

For the 2D conditions, equation (22) is re-written in the form of Relation (23):

$$\begin{bmatrix} k_1^{(c)} \\ k_2^{(c)} \end{bmatrix} = \lambda(1-\alpha_0)\begin{bmatrix} P_1 \\ P_2 \end{bmatrix} \qquad (23)$$

Based thereon, Relation (24) is concluded:

$$\begin{bmatrix} k_1^{(c)} \\ \overline{k_2^{(c)}} \end{bmatrix}\begin{bmatrix} P_1 \\ \overline{P_2} \end{bmatrix} = 1 \qquad (24)$$

The parameters have been specified before-hand.

4. Results

To calculate the fracture tensor, the first step is clustering and determining the set of the joints in the studied region. In this stage, the statistical analysis of the collected data based on their orientation indicators enables clustering of the collected data in certain sets. Table 1 summarizes the results of the statistical analysis and classification of the collected data.

Table 1. Results of statistical analysis of surveyed data from the cavern.

Joint sets		Dip Direction (°)	Dip (°)	K-Fisher	Mean trace Length (cm)	S.D. of trace length (cm)
First set		123	60	17.3	64.1	53
Second set		280	46	9.5	66.5	53.4
Bedding	Parents	33	76	25.6	892	300
	Daughters	29	73	10.4	221.57	107.7

It can be seen from Table 1 that the collected data can be classified into four sets according to their conditions. It is worth mentioning that the sampled strata fall in one set in terms of dip and dip direction but they are dividable into two separate sets of parents and daughters in terms of the collected impact lengths. After statistical analysis of the collected data and determining the fracture sets, the orientation tensor of each joint-set is calculated. In computing the orientation tensor of each joint set, use will be made of the cumulative density of the region wherein the fracture is situated. Table 2 shows the orientation tensor calculated for each joint set. In computing the orientation tensor of the joint set, use will be made of the cumulative density of the region wherein the fracture is situated plus the normal vector of each fracture, as well.

Table 2. Orientation matrix which is calculated for each joint set.

Joint sets	Orientation tensor
First set	$\begin{bmatrix} 0.163 & -0.031 & 0.062 \\ -0.031 & 0.173 & -0.564 \\ 0.062 & -0.564 & 0.364 \end{bmatrix}$
Second set	$\begin{bmatrix} 0.735 & 0.015 & -0.756 \\ 0.015 & 0.038 & 0.711 \\ -0.756 & 0.711 & 0.958 \end{bmatrix}$
Parent	$\begin{bmatrix} 0.497 & 0.159 & -0.017 \\ 0.159 & 0.098 & -0.356 \\ -0.017 & -0.356 & 0.256 \end{bmatrix}$
Daughter	$\begin{bmatrix} 0.467 & -0.824 & -0.005 \\ -0.824 & 0.371 & 0.515 \\ -0.005 & 0.515 & 0.062 \end{bmatrix}$

After calculating the orientation tensor for each joint, the orientation tensor of the entire joint set is calculated based on the superposition principle. Thus in this stage, the orientation tensor of each joint set is calculated for it is considered as one of the parameters required for the calculation of the fracture tensor.

After computing the fractures' orientation tensor, the turn comes for the estimation of the probability distribution function of the fractures' impact length. To estimate the probability distribution of the fractures' impact length, it is necessary after collecting the fractures' impact length rates to make use of various statistical tests like chi square and/or Kolmogorov test and others so that the goodness of fit can be estimated for the various distribution functions over the collected data and the best function with the highest fit index can be eventually selected as the probability distribution function of the impact lengths. The result of estimating the various distribution functions' fit over the fractures is suggestive of the exponential function's match with them.

According to the presented results, it is clear that the exponential distribution function has the best fit over the data related to the fracture impact considering the parameters determined in the table hence it can be considered as the distribution function governing the fractures' impact length. The reason for searching for and estimating the distribution function governing the fractures' impact length is the use of its moments during the process of calculating fracture tensor. The moments required by the probability distribution function of the fractures' impact lengths for the calculation of the fracture tensor are the first and the second moments of the distribution function the calculated values of which for the fractures have been given in Table 3.

Table 3. First and second moments of probability density function of trace length of joints.

Joint set	First moment	Second moment
First set	**64.1**	**0.2809**
Second set	**66.5**	**0.2854**
Bedding (parents)	**892**	**9**
Bedding (daughters)	**221.57**	**1.1449**

In continuation of the fracture tensor calculation process, the normal vector image of each fracture should be obtained along each line. In this stage, after calculating the normal vector image of each fracture along the collection line, all of the normal images of the joints should be summed up for calculating the fracture tensor. After calculating the fractures' sum of the normal vector images along the collection line, the last parameter required for complementing the fracture tensor calculation process is the computation of the fractures' linear density. To do so, it is enough to divide the total number of the fractures intersected by the collection line by the total length of the collection line. If the aforesaid calculation method is applied for the fractures' linear density. Table 4 shows the linear density as well as the calculate sum of the normal vector images of the fractures.

Table 4. Linear density and sum of projections of unit normal of joints.

Joint set	Sum of projections	Linear density
First set	**72.67**	**1.63**
Second set	**74.36**	**1.49**
Bedding (parents)	**91.20**	**1.86**
Bedding (daughters)	**66.69**	**1.97**

Based on the calculations and the obtained required parameters, the fracture tensor can be computed for the collected data and, in fact, the fracture tensor can be calculated for the studied region in Lorestan's Rudbar pumped-storage hydroelectric plant and. It is worth mentioning that using the orientation tensor of each joint set, the fracture tensor of each fracture set can be obtained. After calculating the fracture tensor of each joint set, the superposition principle can be applied to compute the total fracture tensor of the entire fractures. The fracture tensors of each joint set as well as the calculated output fracture tensors of the studied region have been given in Table 5.

Table 5. Calculated crack tensor for each joint set.

Joint set	Crack tensor
First set	$\begin{bmatrix} 4.7174 & 1.287 & 2.957 \\ 1.287 & 3.6968 & 0.844 \\ 2.957 & 0.844 & 0.5035 \end{bmatrix} \times 10^{-7}$
Second set	$\begin{bmatrix} 4.195 & 1.158 & 2.142 \\ 1.158 & 2.4124 & 0.9696 \\ 2.142 & 0.9696 & 0.2679 \end{bmatrix} \times 10^{-7}$
Bedding (parents)	$\begin{bmatrix} 2.629 & 0.0294 & 2.789 \\ 0.0294 & 2.6087 & 0.5804 \\ 2.789 & 0.5804 & 0.5118 \end{bmatrix} \times 10^{-7}$
Bedding (daughters)	$\begin{bmatrix} 6.897 & 0.965 & 1.421 \\ 0.965 & 2.9563 & 1.668 \\ 1.421 & 1.668 & 0.7673 \end{bmatrix} \times 10^{-7}$
Resultant crack tensor	$\begin{bmatrix} 18.439 & 3.4304 & 9.3102 \\ 3.4304 & 11.6742 & 4.0616 \\ 9.3102 & 4.0616 & 2.0506 \end{bmatrix} \times 10^{-7}$
Principal components of resultant	$\begin{bmatrix} 24.4746 & 0 & 0 \\ 0 & 10.2404 & 0 \\ 0 & 0 & 2.5511 \end{bmatrix} \times 10^{-7}$

After calculating the fracture tensor, the turn comes for calculating the permeability tensor. To compute the permeability tensor using fracture tensor, Kronecker's delta as well as a constant

should be used that depends on the fracture surface. Considering the calculated fracture tensor, the amount of the studied region's permeability tensor is obtained as given in Table 6, along with the values of the parameters required for its calculation.

Table 6. Mean calculated permeability tensor based on crack tensor.

λ	$\frac{1}{12}$
Mean permeability tensor	$\begin{bmatrix} 17.215 & 0 & 0 \\ 0 & 12.628 & 0 \\ 0 & 0 & 3.816 \end{bmatrix} \times 10^{-7}$
Mean value of permeability	$11.220 \times 10^{-7} \frac{m}{s}$

Besides being computable using fracture tensor, the permeability can also be found by other methods, as well. In this section of the article, validation process is carried out using permeability rate obtained based on fracture tensor and comparing it with the amount of the region's measured permeability. The measured permeability value has been obtained using Lugeon test. The in-situ tests based on Lugeon Method constitute one of the most credible methods and scales for determining permeability and they can also be applied in estimating the subsidence, as well. The permeability rate obtained based on in-situ Lugeon test is equal to $9.23 * 10^{-7}$ m/s. Comparison of the calculated and the measured permeability is indicative of the acceptability of the calculated value. It should be mentioned that because of this fact that the only permeability test which is conducted in the project site was lugeon test, there was no access to other measurements of permeability and for more and accurate study, may be better to compare the result with data that obtain from furthermore measurements. In comparing average value of principal components of permeability tensor and lugeon test data should be noticed that the three value of principal component one by one should be in around of data that is obtained from lugeon test. In detail it is better to compare the value of principal component that directionally is near to the direction of borehole that lugeon test is conducted in. In this work, third component of 3.816×10^{-7} is directionally near value.

5. Conclusions

The effect of fractures on the various behaviors of the rock mass is inevitable. Rock mass permeability is one of the most important characteristics of the rock mass that plays an essential role in designing of various kinds of structures constructed on a mass of rock and it is always taken into consideration in the structures' modeling in terms of stability analysis. Due to the rock masses' anisotropy and inhomogeneity, a tensor quantity is employed for describing its permeability. Thus, calculation of the rock mass permeability tensor is amongst the most important parts of elaborating the ambiguities existent in the maximally precise recognition of the rock mass hence designing of structures featuring high stability and cost-effectiveness. Considering the importance of the subject, there are numerous methods designed for calculating the permeability tensor. Amongst the various kinds of the proposed methods for calculating the permeability tensor, the calculation method using fracture tensor, despite its mathematical complexities, is the only available method that directly applied the fractures' geometrical specifications in calculating the permeability tensor. Unlike the other suggested methods, this method directly calculates the permeability tensor of the rock mass itself and this is quite opposite to the other methods that calculate permeability for the reproduced network of fractures. According to the method's high capability, the permeability tensor was obtained for Rudbar Lorestan pumped-storage hydroelectric plant and dam through calculation of the fracture tensor and it was made clear following its comparison with the measured amount of permeability that it gives better results. It is worth mentioning that the field data were collected from the aforementioned project site for the calculation of the fracture tensor hence the permeability tensor. Besides being applicable to the calculation of permeability tensor, the fracture tensor is also employed in computing the other various behaviors of the rock mass. The extensiveness of fracture tensor's use in various kinds of rock mechanics is reflective of the high importance of its calculation and its availability in various kinds of projects engaged with rock masses.

References

[1]. Kulatilake, P.H.S.W. *et al.* (1993) Effect of finite size joints on the deformability of jointed rock in three dimensions. *Int. J. Rock Mech. Min. Sci. Geomech. Abstr.* 30, 479–501.

[2]. Oda, M. (1982) Fabric Tensor for Discontinuous Geological Materials. *Soils Found.* 22, 96–108.

[3]. Oda, M. (1984) Similarity rule of crack geometry in statistically homogeneous rock masses. *Mech. Mater.* 3, 119–129.

[4]. Oda, M. (1985) Permeability tensor for discontinuous rock masses. *https://doi.org/10.1680/geot.1985.35.4.483* 35, 483–495

[5]. Panda, B.B. and Kulatilake, P.H.S.W. (1995) Study of the effect of joint geometry parameters on the permeability of jointed rockOnePetro

[6]. Kulatilake, P.H.S.W. *et al.* (1996) Box Fractal Dimension And the First Invariant of Fracture Tensor of Fracture Networks As Measures of Statistical Homogeneity of Jointed Rock MassesOnePetro.

[7]. Wang, M. *et al.* (2002) Estimation of REV size and three-dimensional hydraulic conductivity tensor for a fractured rock mass through a single well packer test and discrete fracture fluid flow modeling. *Int. J. Rock Mech. Min. Sci.* 39, 887–904.

[8]. Oda, M. (1986) An equivalent continuum model for coupled stress and fluid flow analysis in jointed rock masses. *Water Resour. Res.* 22, 1845–1856.

[9]. Oda, M. *et al.* (1986) A crack tensor and its relation to wave velocity anisotropy in jointed rock masses. *Int. J. Rock Mech. Min. Sci. Geomech. Abstr.* 23, 387–397.

[10]. Oda, M. (1983) A method for evaluating the effect of crack geometry on the mechanical behavior of cracked rock masses. *Mech. Mater.* 2, 163–171.

[11]. LIAKOPOULOS, A.C. (1965) DARCY'S COEFFICIENT OF PERMEABILITY as SYMMETRIC TENSOR of SECOND RANK. *Int. Assoc. Sci. Hydrol. Bull.* 10, 41–48.

[12]. Asadi, M. *et al.* (2000) Anisotropic Permeability Measurement of Porous Media: A 3-Dimensional Method. DOI: 10.2118/59396-MS.

[13]. Greenkorn, R.A. *et al.* (1964) Directional Permeability of Heterogeneous Anisotropic Porous Media. *Soc. Pet. Eng. J.* 4, 124–132.

[14]. Long, J.C.S. and Witherspoon, P.A. (1985) The relationship of the degree of interconnection to permeability in fracture networks. *J. Geophys. Res. Solid Earth* 90, 3087–3098.

[15]. Min, K.B. *et al.* (2004) Determining the equivalent permeability tensor for fractured rock masses using a stochastic REV approach: Method and application to the field data from Sellafield, UK. *Hydrogeol. J.* 12, 497–510.

[16]. Zhang, F. *et al.* (2004) Determining the Permeability of Fractured Rocks Based on Joint Mapping. *Groundwater* 42, 509–515.

[17]. de Dreuzy, J. *et al.* (2001) Hydraulic properties of two-dimensional random fracture networks following a power law length distribution: 2. Permeability of networks based on lognormal distribution of apertures. *Water Resour. Res.* 37, 2079–2095.

[18]. Hestir, K. and Long, J.C.S. (1990) Analytical expressions for the permeability of random two-dimensional Poisson fracture networks based on regular lattice percolation and equivalent media theories. *J. Geophys. Res. Solid Earth* 95, 21565–21581.

[19]. Zimmerman, R.W. and Bodvarsson, G.S. (1996) Hydraulic conductivity of rock fractures. *Transp. porous media* 23, 1–30.

20. Snow, D.T. (1969) Anisotropie Permeability of Fractured Media. *Water Resour. Res.* 5, 1273–1289.

[21]. Kiraly, L. (2002) Karstification and groundwater flow. in *Proceedings of the conference on evolution of karst: from Prekarst to Cessation. Postojna-Ljubljana*, pp. 155–190.

[22]. Rocha, C. *et al.* (2005) High-resolution permeability determination and two-dimensional porewater flow in sandy sediment. *Limnol. Oceanogr. Methods* 3, 10–23.

[23]. Zoorabadi, M. *et al.* (2012) A new equation for the equivalent hydraulic conductivity of rock mass around a tunnel. *Int. J. Rock Mech. Min. Sci.* 54, 125–128.

[24]. Pan, J.-B. *et al.* (2010) Application of fracture network model with crack permeability tensor on flow and transport in fractured rock. *Eng. Geol.* 116, 166–177

[25]. Rutqvist, J. *et al.* (2013) Linked multicontinuum and crack tensor approach for modeling of coupled geomechanics, fluid flow and transport in fractured rock. *J. Rock Mech. Geotech. Eng.* 5, 18–31.

[26]. Brown, S.R. and Bruhn, R.L. (1998) Fluid permeability of deformable fracture networks. *J. Geophys. Res. Solid Earth* 103, 2489–2500.

محاسبه تانسور نفوذپذیری مغار نیروگاه تلمبه ذخیره‌ای سد رودبار لرستان با استفاده از تانسور ترک

اکبر اسمعیل زاده[1*]، کوروش شهریار[2]، و رضا میکاییل[1]

1. گروه مهندسی معدن، دانشکده محیط زیست، دانشگاه صنعتی ارومیه، ارومیه، ایران
2. بخش معدن، دانشکده معدن و متالورژی، دانشگاه صنعتی امیرکبیر، تهران، ایران

ارسال 2023/02/08، پذیرش 2023/08/07

* نویسنده مسئول مکاتبات: a.esmailzadeh@uut.ac.ir

چکیده:

مشخصه‌های هیدرولیکی توده سنگ، از اهمیت بالایی در تحلیل رفتاری و پایداری سازه‌ای احداث شده در و یا روی توده سنگ هستند. در میان مشخصه‌های هیدرولیکی توده سنگ، نفوذپذیری از مهم ترین پارامترهای آن محسوب شده که نقش کلیدی در رفتار کلی توده سنگ دارد. بر همین اساس پژوهشگران حوزه مکانیک سنگ تلاش‌های زیادی در محاسبه و دسترسی به نفوذپذیری توده سنگ انجام داده‌اند. برای دسترسی به مقدار نفوذپذیری توده سنگ می‌توان از تکنیک های برجا و تکنیک‌های شبیه سازی بهره برد. تست‌های برجا مانند تست لوژن تست‌هایی هزینه بر و زمان‌بر بوده و گاهاً تعمیم نتایج آن به بخش بزرگتری از محدوده تست با چالش‌های اساسی روبه‌رو است. در تکنیک‌های شبیه سازی نیز در واقع نفوذپذیری برای یک مدل محاسبه می‌شود که علارغم شباهت‌های زیاد می‌تواند تفاوت‌هایی را نیز با محیط واقعی داشته باشد و در این مورد نیز استفاده از نتایج شبیه سازی برای محدوده واقعی همراه با احتیاط‌هایی خواهد بود. با در نظر گرفتن دلایل فوق، دسترسی مستقیم به مقدار نفوذپذیری توده سنگ با صرف هزینه و زمان بهینه، که بتوان نتایج آن را برای محدوده معینی بدون چالش تعمیم داد، می‌تواند بسیار ارزشمند باشد. بر همین اساس در این کار پژوهشی با استفاده از مفهوم تانسور ترک، تانسور نفوذپذیری مغار نیروگاه سد رودبار لرستان بطور مستقیم با استفاده از مشخصه‌های ساختاری توده سنگ، محاسبه شده است. بعد از انجام محاسبات، مقدار به‌دست آمده برای نفوذپذیری برابر با 11.220×10^{-7} متر بر ثانیه شده که در مقایسه با مقدار اندازه‌گیری شده توسط تست لوژن که برابر با 9.87×10^{-7} متر بر ثانیه است، مقداری قابل قبول محسوب می شود.

کلمات کلیدی: تانسور ترک، تانسور نفوذپذیری، نیروگاه تلمبه ذخیره‌ای، رودبار لرستان.